

Shrimp: A Robust Underwater Visible Light Communication System

Chi Lin^{1,2}, Yongda Yu^{1,2}, Jie Xiong³, Yichuan Zhang^{1,2}, Lei Wang^{1,2,*}, Guowei Wu^{1,2}, Zhongxuan Luo^{1,2}

¹School of Software, Dalian University of Technology, China

²Key Laboratory for Ubiquitous Network and Service Software of Liaoning Province, China

³University of Massachusetts Amherst, USA

Abstract

This paper presents the design, implementation, and evaluation of *Shrimp*, an underwater visible light communication (VLC) system. To address the unique issues in underwater environment such as water flow and scattered sunlight interference, we exploit the circularly polarized light (CPL) and double links for underwater VLC transmission. A coding scheme tailored for underwater communication based on double CPL design is developed. We prototype *Shrimp* on commercial-off-the-shelf (COTS) LEDs with fabricated printed circuit boards (PCBs). Extensive experiments conducted in an indoor water pool, a lake, and the sea demonstrate that *Shrimp* can combat against environmental interference and achieve robust communication in underwater environments. The communication distance can be up to 3 m in sea/lake water using a 3 W commodity LED, outperforming the VLC schemes designed for in-air communication.

CCS Concepts

- Networks → Network experimentation.

Keywords

Visible light communication, underwater communication, circularly polarized light, robustness, design, implementation

ACM Reference Format:

Chi Lin, Yongda Yu, Jie Xiong, Yichuan Zhang, Lei Wang, Guowei Wu, Zhongxuan Luo. 2021. *Shrimp: A Robust Underwater Visible Light Communication System*. In *The 27th Annual International Conference On Mobile Computing And Networking (ACM MobiCom '21), October 25–29, 2021, New Orleans, LA, USA*. ACM, New York, NY, USA, 13 pages. <https://doi.org/10.1145/3447993.3448616>

*Lei Wang is the corresponding author (Email: lei.wang@ieee.org).

Permission to make digital or hard copies of all or part of this work for personal or classroom use is granted without fee provided that copies are not made or distributed for profit or commercial advantage and that copies bear this notice and the full citation on the first page. Copyrights for components of this work owned by others than ACM must be honored. Abstracting with credit is permitted. To copy otherwise, or republish, to post on servers or to redistribute to lists, requires prior specific permission and/or a fee. Request permissions from permissions@acm.org.

ACM MobiCom '21, October 25–29, 2021, New Orleans, LA, USA

© 2021 Association for Computing Machinery.

ACM ISBN 978-1-4503-8342-4/21/10...\$15.00

<https://doi.org/10.1145/3447993.3448616>

1 Introduction

Underwater wireless communication can enable a wide range of commercial and military applications. In recent years, a considerable amount of effort has been devoted to developing efficient underwater communication technologies. Due to severe attenuation in water, radio frequency (RF) signals (e.g., WiFi and LTE), which have achieved great successes in through-air communication, are not suitable for underwater communication. Take WiFi as an example, the attenuation of the 2.4 GHz WiFi signals in the seawater can be as high as 169 dB per meter [26], leading to a limited half meter transmission range. To reduce the attenuation of RF signals, researchers employ RF signals at a very low frequency band (3–30 kHz) for transmissions [72]. Although the signal transmission range can be increased, the channel bandwidth and the data rate significantly decrease. Furthermore, to efficiently receive such low frequency RF signals, the antenna size needs to be huge,¹ and these large-size antennas are usually only used in submarines [65]. These limitations greatly constrain the applicability of RF signals in underwater communication.

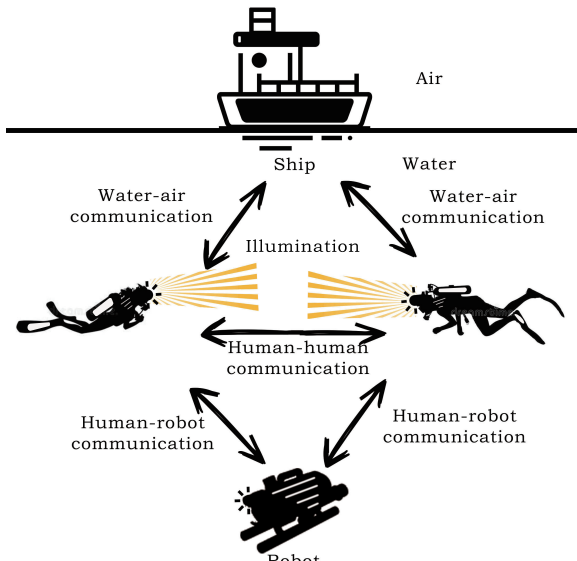


Figure 1: A system overview of *Shrimp*. The dive light is employed for simultaneous communication and illumination.

¹The antenna size needs to be larger than 1/4 of the signal wavelength for efficient signal reception.

The most popular underwater communication technologies are based on acoustic signals [56], i.e., underwater acoustic communication (UAC), which can effectively transmit signals to kilometers away. However, some intrinsic drawbacks such as low data rate and large latency make UAC unsuitable for high speed and real-time communication systems.

To address these issues, underwater optical wireless communication (UOWC) is proposed. In particular, laser-based communication systems [15, 49] have attracted lots of attention owing to their high data rates. However, shortcomings still exist, preventing them from wide adoptions. First, laser communication relies on precise beam alignment between the transmitter and receiver due to laser's high directionality. However, in an underwater environment, the water flows can cause device displacements, making it difficult to achieve a tight device alignment. It is also challenging to employ laser signals for underwater human-human communication due to human's mobility. Second, the laser beam has a very high energy density, which may cause harm to human eyes and body tissues when laser beam is used for human-robot and human-human communication. Besides, the hardware module for laser communication is usually expensive.

In recent years, visible light communication (VLC) technology has shown promising merits in terms of latency, cost, and data rate. The transmission rate is not as high as that of the laser-based approaches [15] but is good enough for a large range of applications [25]. Although VLC technology does not require a tight transceiver alignment, the device rotation/displacement² caused by water waves can still undermine the transmission performance. Furthermore, the severe attenuation in water and highly dynamic sunlight interference, all bring in new challenges for underwater VLC. Thus, we need a new VLC design for complicated underwater environment in the wild. It requires the system to tolerate transceiver rotation/displacement and deal with dynamic sunlight interference.

The goal of this paper is to develop an underwater VLC system based on cheap commercial-off-the-shelf (COTS) LEDs, achieving the following objectives.

Portable and low cost. Since the proposed system is designed for underwater environment, it is preferred the system has a small size and a light weight. In such a case, users can easily carry it without incurring a burden.

Can work robustly in harsh underwater environment. The proposed system should not require strict device alignment and should be robust against dynamic sunlight interference.

Does not compromise the illumination function. We would like the proposed system to achieve robust data transmission without compromising the LED's illumination function.

To achieve these goals, we need to tackle several challenges related to unique underwater environment.

- The continuous water flows move/rotate the transmitter and receiver, which can affect the data transmission of light-based communication systems. Thus, *achieving reliable communication that can tolerate transceiver displacement/rotation in underwater environment* is the first challenge.

²From our experiments, in underwater environment, device rotation and displacement usually occur at the same time with water flows.

- The sunlight interference can be strong in underwater environment. The water waves can scatter the sunlight, which produces severe interference for underwater VLC. What makes it worse is that compared to the relatively stable sunlight interference in the air, the intensity of the scattered light keeps changing. The intensity variation can span up to two orders of magnitude. Therefore, *addressing the dynamic ambient sunlight interference in underwater environment* is the second challenge.
- When visible light propagates in the air, the reflection is very little. However, due to water flow and uneven salinity, the reflection in seawater is more severe, attenuating the received signal and accordingly causing larger bit error rates (BERs) and shorter transmission distance. Consequently, the third challenge is *increasing the communication distance in underwater environment*.

To tackle the aforementioned challenges, we design and implement an underwater VLC system, named *Shrimp*³ based on COTS LEDs in this work. As shown in Figure 1, the light source (LEDs) can be used for both illumination and communication in *Shrimp*, which lays a basis to enable human-robot, human-human, and water-air communication. Specifically, we exploit the circularly polarized light (CPL) for underwater VLC transmission to deal with the device displacement/rotation issue [13, 77]. Furthermore, to combat sunlight interference, we construct two communication links in which CPL of opposite rotation directions (counterclockwise and clockwise) are used. Besides, a bipolar coding scheme tailored for two CPL links, termed *UBC* is designed to increase the communication distance.

Comprehensive experiments demonstrate that the proposed system is able to combat against dynamic sunlight interference and wave-induced device rotation/displacement, achieving robust performance in underwater environments. Another appealing advantage of the proposed system is that the proposed system can achieve NLoS (non-line-of-sight) communication by reflection, which increases the size of the coverage area and provides a new communication paradigm when the LoS (line-of-sight) path is blocked. In general, the contributions of this paper are summarized as follows.

- (1) We exploit a double CPL (counterclockwise and clockwise CPL) scheme for underwater visible light communication, which can greatly enhance the system robustness. More specifically, the CPL design is robust against transceiver displacement/rotation, and the double CPL design helps to deal with the dynamic sunlight interference in underwater environment. We also propose a coding scheme *UBC*, which is catered for the double CPL design. The coding design helps to increase the communication distance in underwater environment.
- (2) We implement *Shrimp* using cheap commodity hardware such as the COTS dive lights. We design and fabricate printed circuit boards (PCBs) to remedy the limited sensitivity of the cheap silicon photodiode adopted at the receiver. We also

³In the ocean, the mantis shrimp can detect circularly polarized light and use it as a private link for communication, which is similar to the proposed system. Thus, we name the proposed system *Shrimp*.

- hack the LED driver to control the LED circuits for a higher ON/OFF rate.
- (3) Comprehensive experiments are conducted in different underwater environments, including an indoor water pool, a lake, and the sea to validate the effectiveness of *Shrimp*.

2 System Overview

The system architecture of *Shrimp* is shown in Figure 2. On the hardware side, we design and prototype the transmitter and receiver. For the transmitter, we employ cheap commodity LEDs and make modifications to the driver circuit to increase the ON/OFF rate and tune the light intensity for data encoding. For the receiver, we fabricate a PCB to remedy the low sensitivity of the silicon photodiode and employ a differential amplifier to remove the common interference and noise at the two CPL links.

At the transmitter side, the data is first encoded using the proposed *UBC* scheme and then passed to the two transmitter front ends (Tx1 and Tx2), each of which is equipped with an LED, a linear polarizer and a quarter-wave plate as depicted in Figure 2. The two linear polarizers are orthogonal to each other (90° and 0°). With linear polarizers and quarter-wave plates, the two front ends emit circularly polarized light in opposite directions (counterclockwise and clockwise).

At the receiver side, there are also two front ends (Rx1 and Rx2), each is composed of an optical filter, a quarter-wave plate, a linear polarizer, and a silicon photodiode. Similarly, the angles of the linear polarizers at Rx1 and Rx2 are also orthogonal to each other (0° and 90°) as shown in Figure 2.

Therefore, two communication links are established: Link 1 (Tx1-Rx1) and Link 2 (Tx2-Rx2). These two links are nearly identical except the angle of polarizers. Upon reception of light signals at Rx1 and Rx2, an I-V amplifier is used to remedy the limited sensitivity of the cheap silicon photodiode adopted at the receiver. After that, a differential amplifier is utilized to remove the common interference and noise at the two links. Finally, the data is decoded at the receiver side.

The advantages of the *Shrimp* design are twofold. Compared with LPL⁴ design, the CPL design can tolerate device displacement/rotation. It mitigates the misalignment issue caused by water flow or user mobility in underwater communication. Hence, the tight alignment of transmitter and receiver is not required. The design of “double” CPL links has advantages in combating dynamic environmental interference. The reason is that in *Shrimp*, two CPL links are physically close to each other (see Figure 9(a)). Therefore, the environmental interference such as the ambient sunlight contained in these two links are similar, and a differential amplifier can be adopted to remove the common interference. Hence, the double CPL design can help to achieve reliable communication in the presence of strong dynamic interference and device displacement/rotation, which are unique challenges in underwater environment.

⁴Although unpolarized light can also tolerate device displacement/rotation, the interference on unpolarized light is more severe because sunlight is also unpolarized. The interference from the unpolarized sunlight on CPL is less.

3 System Design

In this section, we present the detailed system design, which starts with the design of the transmitter followed by the receiver design.

3.1 Transmitter Design

The transmitter is responsible for encoding data and converting unpolarized light emitted from LEDs into circularly polarized light.

At the transmitter end, we use a COTS LED to emit unpolarized natural light. Then linear polarizers and quarter-wave plates are used to convert unpolarized light into linearly polarized light (LPL) first and then circularly polarized light (CPL). The key here is to modify cheap COTS LEDs for transmission and select appropriate polarizers and waveplates for state conversions of the light signal. The theoretical derivation of the light signal state conversions can be found in the Appendix.

• **Hardware Design and Modification.** To maintain a low cost, we implement the transmitter by modifying a cheap dive light (about \$1). A dive light is composed of two main parts: a light emitting diode (LED) and a driver circuit as shown in Figure 3. The LED is responsible for emitting unpolarized light while the driver circuit controls the current and voltage of the LED. The main purpose of the driver circuit is to control the light ON/OFF rate and tune the duty cycle of the pulse-width modulation (PWM) scheme. We modify the driver circuit to increase the light ON/OFF rate to achieve a higher data transmission rate.

For PWM modulation, two parameters characterize its behavior: duty cycle and frequency. The duty cycle describes the percentage of time the signal is in the ON state of a full cycle. The frequency determines how fast the PWM scheme completes a cycle (e.g., 100 Hz means each cycle completes in 0.01 second). Because there is only one transition in each cycle, the frequency also determines how many light ON/OFF transitions are there in one second. In VLC system design, flickering is a prominent issue needs to be addressed as it causes unsatisfactory user experiences and is harmful to human eyes. To deal with the flickering issue, a higher than 100 Hz ON/OFF frequency is usually required [64]. This is easily satisfied if there are no long consecutive ON (or OFF) states because most commodity LEDs employ a PWM frequency higher than 20 kHz to avoid audible acoustic noise generated due to vibration of the ceramic capacitor widely used in LED driver circuit [20].

Table 1: PWM frequency of three LEDs.

LED	LED driver	Illumination	Maximum
Cree XHP-70	Cree Driver	20 kHz	120 kHz
Cree XHP-50	Cree Driver	20 kHz	200 kHz
Cree XM-L	PT4115	50 kHz	500 kHz

LED is originally designed for illumination. We now explore the potential of utilizing commodity LEDs for data communication by hacking three commonly seen LED driver circuits. Our purpose is to measure the current and voltage features of the driver, which will provide us the basis to modify the commodity LED to realize VLC functionality. We find that, when these LEDs are used for illumination, the control current in the driver is less than 25 mA [5]. Such

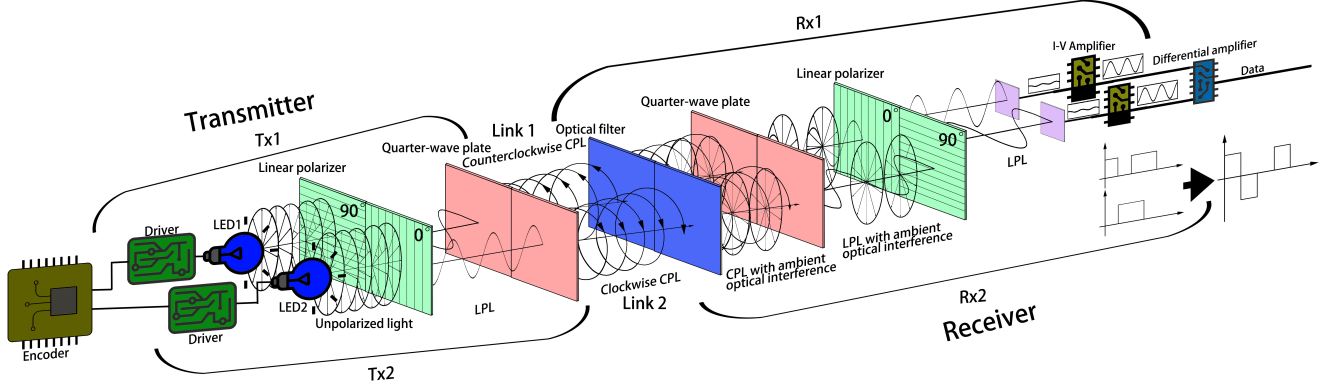
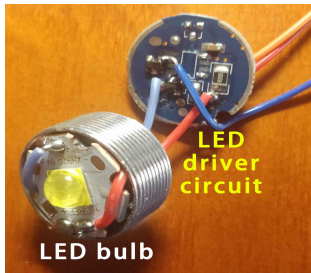
Figure 2: System architecture of *Shrimp*.

Figure 3: The two key components of a dive light: an LED bulb and the associated LED driver circuit.

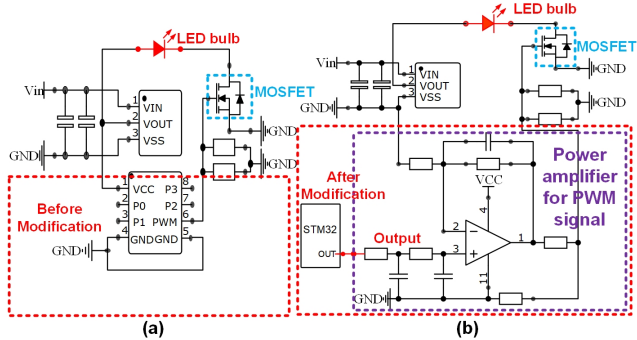


Figure 4: The circuit design of the dive light: (a) before and (b) after modification.

a small current cannot support super quick charge and discharge of the Metal-Oxide-Semiconductor Field-Effect Transistor (MOSFET) [42]. Therefore, the maximum frequency for PWM is limited to 20 kHz as shown in Table 1 [2–4]. Surprisingly, we find that by simply increasing the control current, the maximum possible PWM frequency can be increased to be significantly larger than 20 kHz. Hence, in our hardware design, we employ the STM32 Microcontroller Unit (MCU) as the signal generation chip and use a power

amplifier (the purple dotted region in Figure 4(b)) to amplify the output current to 100 mA.⁵ Accordingly, a larger current can support a higher frequency of charging and discharging the MOSFET. With this simple modification, the maximum PWM frequency can be increased to 120 kHz, enabling us to increase the VLC transmission rate. For the other two LEDs, the maximum PWM frequency can be increased to 200 kHz and 500 kHz, respectively.

• Circularly Polarized Light (CPL) and Polarizers.

Now we describe how to generate CPL for communication. In the proposed system, polarizers and waveplates are used to convert the unpolarized light into linearly polarized light first and then into circularly polarized light. The reason why we use CPL for underwater communication rather than linearly polarized light is that the CPL design does not require tight transceiver alignment in underwater communication. Moreover, the double CPL links show unique merits in eliminating the ambient light interference. We present the detailed reasons below.

While unpolarized light works well in the air in indoor environment, it is not suitable for underwater communication as it can easily be interfered by strong outdoor ambient light which is also unpolarized. When linearly polarized light (LPL) is used for communication, as the electrical field of the light is confined in a single plane, it requires spatial alignment of the transmitter and receiver. When there is a rotation with the transceivers, the transmission can get affected. In underwater environment, continuously fluctuating waves can easily move the transceivers, making it difficult or even impossible to achieve tight transmitter-receiver alignment. On the other hand, CPL can overcome this issue. Different from LPL whose electrical field is restricted in one plane at one direction, CPL's electrical fields are in all the directions perpendicular to the direction of propagation. Therefore, the device rotation has little effect on the transmission link. This unique feature of CPL is thus adopted to address the alignment issue in underwater environment. The relationships between the unpolarized light, LPL, and CPL are shown in Figure 5.

⁵The adopted amplifier can only support a maximum current of 100 mA. We believe with more advanced hardware, this current can be further increased.

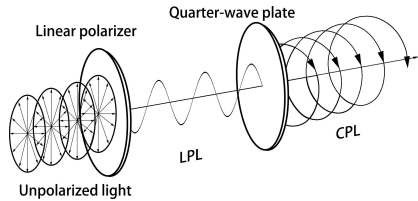


Figure 5: From unpolarized light to circularly polarized light (CPL).

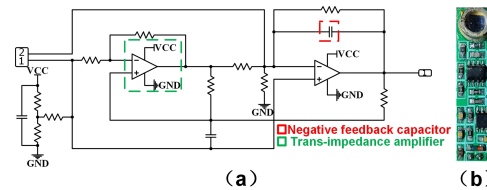


Figure 6: (a) The detailed design and (b) PCB implementation of the I-V amplifier.

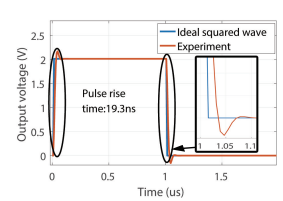


Figure 7: Signal waveform is affected little after going through the I-V amplifier.

3.2 Receiver Design

For the implementation of the receiver, we use a COTS silicon photodiode to capture the arriving light signal and convert it into electrical current signal. However, limited by the intrinsic feature of the photodiode, the output current is usually weak. For example, when the power intensity of the incident light is 1000 W/m^2 , the output current of the silicon photodiode is around 900 nA. Such a weak current can be corrupted by hardware noise, causing errors in decoding. To address this problem, an I-V amplifier is designed and fabricated to amplify this current. We utilize a negative feedback capacitor to reduce the noise of the output signal. The design and implementation of our amplifier are shown in Figure 6(a) and (b) respectively. We fabricate PCB for this circuit and test its performance. As shown in Figure 7, the edge rising time is only 19.3 ns, which occupies about 1.93% of a cycle. This result demonstrates that the waveform of the signal is affected very little after going through the I-V amplifier.

Another issue we need to address is that the received CPL signal in each link contains not only the expected signal but also environment-induced interference. The intensity of the dynamic ambient sunlight interference can span up to two orders of magnitude and keeps changing over time, which is non-trivial to be removed. Owing to the two-link design, the environment-induced interference in the two links are very similar because Tx1-Rx1 and Tx2-Rx2 are physically close to each other. Note that even the interference keeps changing, the changes are similar at the two links and can therefore still be mitigated using the differential amplifier. We apply an AD620 differential amplifier [1] to remove the common interference at both links in our design.

Hardware cost and size. The hardware costs include the following: two sets of LEDs and fabricated PCBs (\$11), polarizers and films (\$12), silicon photodiodes (\$3), I-V amplifier and differential amplifier (\$40), and waterproof cover and glue (\$11), which lead to a total cost of about \$77. The size of the device is $9 \text{ cm} \times 9 \text{ cm} \times 13 \text{ cm}$ with a weight of 326 g (twice the weight of a Samsung S20 smartphone). In general, the designed system has a small size, a light weight, and is also relatively cheap.

4 Coding Scheme

We develop an underwater bipolar coding scheme (*UBC*), which is catered for the double CPL design. We borrow the idea from the High-Density Bipolar of Order 3 (HDB3) coding scheme [53] and make changes. The reason we do not adopt a simpler coding scheme such as the Manchester coding in *Shrimp* is as follows.

Manchester scheme is a simple coding scheme which can avoid flickering. However, the cost is that Manchester scheme sacrifices the data rate. Manchester coding fundamentally is a 1B2B scheme which means every 1 bit of output needs 2 bits of input. More advanced 4B6B, 8B10B [50] codes incur less loss. However, the efficiency is still lower than the *UBC* coding scheme which supports 1 bit of output with 1 bit of input. The trade-off of *UBC* scheme is the more complicated encoding/decoding procedure. As higher data rate and longer distance are the objectives in this work, we adopt the *UBC* scheme rather than the simpler Manchester coding scheme. Another reason we adopt the *UBC* scheme is that there are three states for *UBC* coding (0, -1, and +1) and therefore it well suits the double link design which can support a maximum of four states (00, 01, 10, and 11). Note that in our double link design, we employ the difference of the two links to remove noise and therefore 00 and 11 states present the same 0 state, and accordingly, only 3 states are supported. Thus, the two link design and the *UBC* coding suit each other well. Also, *UBC* scheme has a built-in error detection capability. We present the detail of *UBC* scheme below.

4.1 Encoding

At the transmitter, the encoding scheme consists of two phases: (i) initialization and (ii) bit conversion.

In the *initialization phase*, we use a bipolar scheme to encode binary information, in which bit 0 remains to be encoded as 0, and bit 1 has two representations: positive (+1) and negative (-1). As shown in row 2 of Figure 8(a), in the initialization phase, bit 1 is alternately encoded as +1 and -1. An underlying problem here is that a long chain of consecutive 0s will cause turning OFF LEDs for a period of time, potentially causing flickering [80]. To solve this problem, in *bit conversion* phase, we include two specialized bits: V (violation bit) and B (insertion Bit). The detailed steps are described as follows.

Step 1: Originally, there are a number of consecutive 0s in the data (row 1 in Figure 8(a)). We check whether there are four consecutive zeros. If four consecutive zeros are detected as shown in the red, green, and blue boxes in row 2, the last zero bit will be replaced by a V bit as shown in row 3. After this step, the number of consecutive 0s will be no more than three. By limiting the number of consecutive 0s to be no more than three, we avoid long consecutive 0s. Note that for a very small time interval, the average light intensity varies. When the length of the time interval increases to a relatively large value (e.g., 1 ms), the average light intensity is

Row Index	Operation	Encoding Data																
1	Original	1	0	0	0	0	0	0	0	0	1	1	1	0	0	0		
2	Initialization	+1	0	0	0	0	0	0	0	0	-1	+1	-1	0	0	0		
3	Insert V bit	+1	0	0	0	0	0	0	0	+V	0	-1	+1	0	0	0		
4		+1	0	0	0	0	0	0	+V	0	-1	+1	-1	0	0	+1		
5	Insert B bit	+1	0	0	0	+V	-B	0	0	-V	0	-1	+1	-1	0	0	-V	+1
6		+1	0	0	0	+V	-B	0	0	-V	0	-1	+1	-1	0	0	-V	+1
7	After Encoding	+1	0	0	0	+1	-1	0	0	-1	0	-1	+1	-1	0	0	-1	+1
8	Link 1	+1	0	0	0	+1	-1	0	0	-1	0	-1	+1	-1	0	0	+1	-1
9	Link 2	+1	0	0	0	+1	-1	0	0	-1	0	-1	+1	-1	0	0	+1	-1
10		+1	0	0	0	+1	-1	0	0	-1	0	-1	+1	-1	0	0	+1	-1

Row Index	Operation	Decoding Data																Error	
1	Before decoding	+1	0	0	0	+1	-1	0	-1	+1	-1	0	0	0	-1	-1	-1	-1	
2	Step 1	+1	0	0	0	+1	-1	0	0	-1	0	-1	+1	-1	0	0	0	-1	-1
3		+1	0	0	0	+1	-1	0	0	-1	0	-1	+1	-1	0	0	0	-1	-1
4		+1	0	0	0	+1	-1	0	0	-1	0	-1	+1	-1	0	0	0	-1	-1
5		+1	0	0	0	+1	-1	0	0	-1	0	-1	+1	-1	0	0	0	-1	-1
6		+1	0	0	0	+1	-1	0	0	-1	0	-1	+1	-1	0	0	0	-1	-1
7		+1	0	0	0	+1	-1	0	0	-1	0	-1	+1	-1	0	0	0	-1	-1
8	Step 2	+1	0	0	0	+1	-1	0	0	-1	0	-1	+1	-1	0	0	0	-1	-1
9	After decoding	1	0	0	0	0	0	0	0	0	0	1	1	1	0	0	0	0	0

(a)

(b)

Figure 8: An illustration of the UBC scheme: (a) the encoding process and (b) the decoding process.

almost a constant. The polarity of V is the same as the previous non-zero bit and examples are shown in row 4 of Figure 8(a).

Step 2: After Step 1, there are three consecutive 0s in front of every V bit in row 3. Now, if we find zero or even number of 1s (+1 or -1) between two consecutive V bits (+V or -V), three 0s in front of the latter V will be replaced by B00 as shown in row 5. Here, the polarities of the B bit and the latter V bit are both set as opposite to the polarity of the previous non-zero bit as shown in row 6 in Figure 8(a).

Then, we replace +V and +B (-V and -B) as +1 (-1) to obtain the encoded data, as shown in row 7 in Figure 8(a). We employ the two front ends Tx1 and Tx2 to transmit data in Link 1 and Link 2. Here, bit +1 (-1) is represented by turning ON (OFF) Tx1 and turning OFF (ON) Tx2. Bit 0 is expressed by turning ON both Tx1 and Tx2, as shown in row 8 and row 9 in Figure 8(a). The rotation directions of CPL transmitted in two links are also depicted.

4.2 Decoding

At the receiver end, after applying the differential amplifier to remove the interference, we proceed to decode the data in two steps as shown in Figure 8(b). Step 1 converts the encoded data m into the bipolar coding form m' and checks errors. Step 2 further recovers m' to the original data.

Step 1: To decode data, we traverse from the beginning to the end of the frame. If there are two or three zeros between two identical adjacent non-zero bits (two +1s or -1s), the latter non-zero bit, together with the three bits in front of it, will be replaced by four consecutive 0s. Examples are shown in row 3, 5, and 7 in Figure 8(b).

Step 1 can also be applied to check bit errors. For any same adjacent non-zero bits (two +1s or -1s), if the number of zeros between them is not two or three, we can conclude that among the four bits (i.e., the latter non-zero bit and three bits in front of it), at least one bit is wrong. An example is presented here to demonstrate the error checking capability. As shown in Figure 8(a), the last bit of row 7 should be +1. However, at the receiver end, we receive bit -1. During the decoding process, we can find that the number of zeros between the last two -1s is zero in row 6 of Figure 8(b) rather than two or three. Hence we can infer that there is an error among these four bits which are marked yellow in row 8. Note that UBC is only able to detect errors but not able to correct them.

Step 2: We then proceed to recover the original data. We first handle the polarity of each bit. The polarity of the first non-zero bit should be +1, and the polarities of every two adjacent non-zero

bits are opposite to each other (refer to the examples in row 8 of Figure 8(b)). By applying this rule, the first non-zero bit is +1, the second non-zero bit is -1, and the third non-zero bit is again +1. We continue this process to assign the polarities for all the non-zero bits. Afterwards, we can just remove the polarity of each non-zero bit to recover the original data as shown in row 9 of Figure 8(b).

5 Experiments

We design and prototype *Shrimp*, as shown in Figure 9(a) and (b). We conduct experiments in different environments to evaluate the performance of the proposed system.

5.1 Experiment Setups

Extensive experiments are conducted in different environments, including a 5 m × 3 m × 1 m water pool (Figure 9(f) and (g)), a lake (Figure 9(c) and (e)), and the sea (Figure 9(d), (h) and (i)).⁶ When experiments are conducted in the lake and at the seaside, both transceivers are tied on the 2-meter iron rods (Figure 9(e) and (i)). For deep water experiments (depth > 2 m), we place the transceivers on two underwater robots (Figure 9(c), (d), and (f)). The robots can freely move, float, dive, and rotate in the water. The robots can dive for a depth up to five meters. In our experiments, we use a battery pack to empower the system. The system power consumption is around 20 W. A battery pack with a size of 10000 mAh can enable the system to work for around 3 hours.

5.2 System Performance

We choose OpenVLC [6], a widely adopted VLC research platform for performance comparison. For a fair comparison, we tune the resistor to control the transmission power of *Shrimp* to ensure that the total light intensity of the two links in *Shrimp* is equal to light intensity of the single link of OpenVLC at a same distance from the transmitter. To explore the salient features of light in underwater communication, besides the white color light, we also employ blue color light to study the effect.

• **Performance in the Air.** Although our system is designed for underwater environment, we also would like to evaluate its performance in the air. The first experiment is conducted on the ground with a low ambient light intensity. We measure the achievable data rates at different communication distances. As shown in

⁶The photos in Figure 9(d) and (h) are taken by robots in the sea and thus they are not clear enough due to the relatively low visibility.

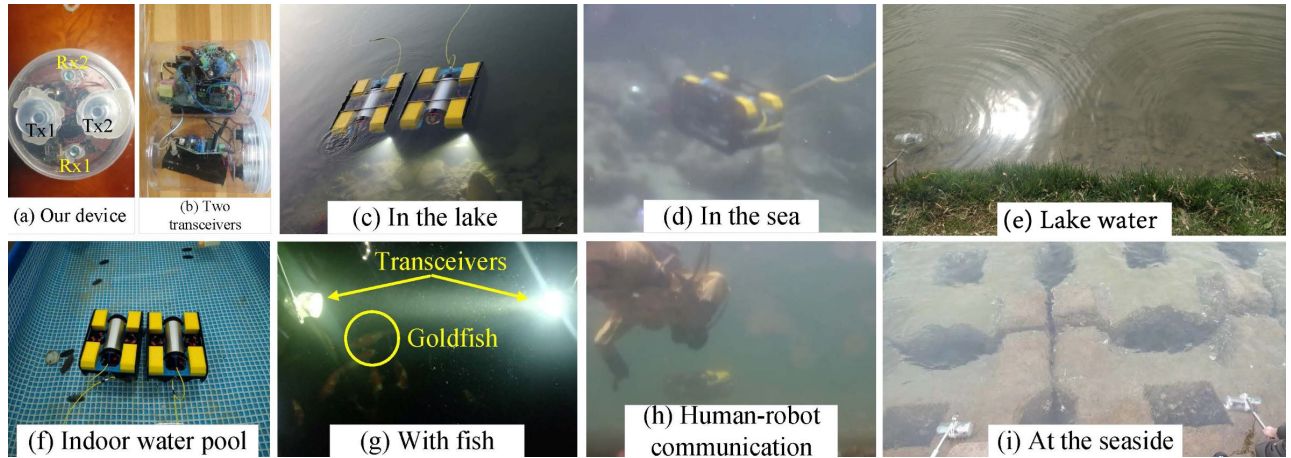


Figure 9: Prototype and different experiment environments.

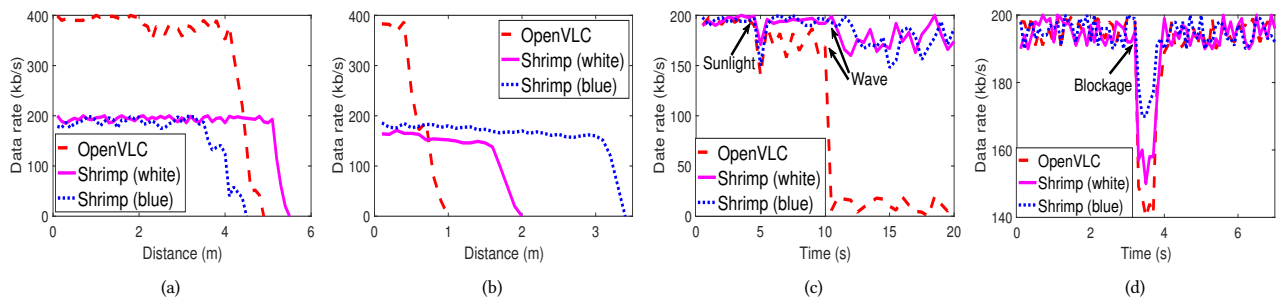


Figure 10: Performance comparison with OpenVLC in different scenarios: (a) in the air; (b) in the lake, (c) with sunlight and waves; and (d) with an obstacle.

Figure 10(a), we can see that the achievable maximum data rate of OpenVLC is around 400 kbps in the air when the communication distance is less than 3.5 meters. Note that when the distance is small, the signal to noise ratio (SNR) is big enough that the deciding factor of the data rate is the light ON/OFF frequency. *Shrimp* achieves a maximum data rate around 200 kbps. This is because different hardware components are adopted. OpenVLC utilizes a programmable real-time unit (PRU) which can support a higher light ON/OFF rate. On the other hand, *Shrimp* achieves a larger transmission range.

We also observe that the white color light achieves a slightly larger transmission rate and a longer transmission distance compared to the blue light. The reason is that the Rayleigh scattering is more severe with shorter wavelength signals in the air [14]. The wavelength of the blue light (450-490 nm) is shorter than the average wavelength of the white light. Thus, blue color suffers from a larger attenuation and accordingly its transmission range is smaller in the air.

- **Performance in the Water.** In underwater environment (Figure 9(c)), the performance of OpenVLC degrades as shown in Figure 10(b). The data rate decreases with an increasing distance. When the distance is around one meter, the data rate is decreased close to 0. On the other hand, benefit from the double CPL design, the proposed system can still achieve a good performance in terms of

data rate and transmission range. When the distance is increased to one meter, the data rate of the proposed system just slightly drops. Interestingly, we find that the blue color light achieves a longer communication distance and a higher data rate in the water, which is different from the result in the air. The communication distance can be up to 3 meters. We believe the main reason is that the sea/lake water is blue/green in color and thus it absorbs less blue and green light. Therefore, when blue/green light penetrates through the water, the energy gets absorbed less compared to other colors. Hence, the blue light achieves a longer communication distance and a higher data rate than the white color light. This interesting observation suggests that in the sea/lake water, we can choose the light with a similar color to that of the water to achieve a better performance in terms of data rate and transmission range.

- **Influences of Sunlight and Water Waves.** Both ambient light and wave-induced device rotation/displacement can affect the data transmission. We hereby conduct experiments to evaluate the robustness of the proposed system in an indoor water pool (Figure 9(f)). In this experiment, the distance between the transmitter and receiver is set as 0.8 m. Note that the transmission rate of OpenVLC significantly decreases in the water as shown in Figure 10(b). When the communication distance is 0.8 m, the data rates of *Shrimp* and OpenVLC in the water are nearly the same (about

150–200 kbps).⁷ We hereby set the distance between the transceiver pair as 0.8 m for a comparison of other factors.

As shown in Figure 10(c), initially we use a wooden plate to block the sunlight. We also make sure there is no wave and thus no device rotation/displacement. In this ideal scenario, both the proposed system and OpenVLC perform well, achieving a transmission rate close to 200 kbps. Note that the achieved data rate in the indoor water pool is higher than that in the lake. We believe it is because the water in the pool is cleaner.

At the 5th second, we remove the plate so the sunlight starts interfering the light communication. In this scenario, the intensity of the ambient sunlight measured at the water surface increases to 25000 ± 5000 lux. Note that when the sunlight penetrates through the water to arrive at the receiver, it gets attenuated. From our measurement, the intensity of sunlight interference at the receiver is comparable to the intensity of the light signal. As shown in Figure 10(c), a dramatic decline appears at the moment when sunlight appears for OpenVLC. Then the data rate gets stable at around 160 kbps. On the other hand, the interference has less effect on the proposed system owing to (i) the circularly polarized light and (ii) the double link design which is capable of removing common interference at the two links. The proposed system can still achieve a data rate close to 190 kbps.

At the 10th second, we employ wave generators to create waves in the water. As shown in Figure 10(c), in this scenario, the performance of OpenVLC is greatly affected (data rate is significantly decreased from 160 kbps to below 10 kbps). This is because the waves change the intensity of the scattered sunlight and a highly dynamic interference further degrades the performance of transmission. Note that as OpenVLC adopts unpolarized natural light for transmission, the transmission is not affected as much as linearly polarized light by device rotation/displacement. For the proposed system, although the data rate fluctuates slightly, an average data rate around 175 kbps is achieved.

- **Communication Link Blocked by Objects.** We now evaluate the system performance when the commutation link is blocked by object(s). We employ fish as the object in this experiment because they can be widely found in water environment. Several goldfishes, each with an approximate size of $30\text{ cm} \times 15\text{ cm} \times 2\text{ cm}$ are involved in this experiment. The fishes swim freely in the pool, and they occasionally block the LoS (line-of-sight) link between the transmitter and receiver. The transceiver pair is separated by 0.8 m and the experiment is conducted in the indoor water pool.

As shown in Figure 10(d), when a fish blocks the LoS link, an obvious decrease in data rate for both systems can be observed. *Shrimp* achieves a slightly higher data rate than OpenVLC. Also the performance of white color light gets affected more compared to blue light. Another observation is that although the LoS link is blocked and the data rate gets decreased, the decrease is not significant. For example, the data rate of blue color light is just decreased from around 200 kbps to 170 kbps and is still far above 0. This result indicates that if the blocking object is not big, light signals can still get diffracted to reach the receiver.

⁷Note that the data rate slightly varies in different types of water.

5.3 BER performance

In this section, we present the detailed bit error rate (BER) performance of the system under varying communication distances. The transmission power is set as 5 W in this experiment. The experiment is conducted in the water of the shallow seaside with fluctuating waves (Figure 9(i)). Detailed experiment configurations, otherwise stated, are identical to those in the previous experiments.

As shown in Figure 11, the BER increases with the increment of distance. The BER is lower than 10^{-2} when the transmission range is 3 m. We also note when the BER value is at a low level (10^{-6} - 10^{-4}), it varies due to hardware noise. We also conduct same experiment in the water at the lakeside (Figure 9(e)) and similar results are obtained.

5.4 Evaluation of the Design Components

Now we zoom in to study the effect of the individual design components on the performance.

- **CPL vs. LPL vs. Unpolarized Light.** To demonstrate the advantages of CPL over LPL, we compare the performance of *Shrimp* when it is implemented with and without waveplate (i.e., CPL vs. LPL). The key difference between CPL and LPL is that a slight rotation of the transceiver will lead to link misalignment when LPL is used, which is not an issue for CPL.

One underwater robot is employed for the experiment and we record the inclination angle during the whole process by using a Gyro sensor equipped with the robot. The readings from the Gyro sensor indicate that the robot's inclination angle can be up to 30° in the water caused by continuous waves.

We then compare the BER of LPL and CPL at different robot inclination angles. The distance between the transmitter and receiver is kept as 0.8 m. As shown in Figure 12, for LPL, when the inclination angle reaches 12° , a large BER occurs and the BER keeps increasing when the inclination angle increases. On the other hand, when CPL is employed, the BER stays at a low level and is only very slightly affected even when the inclination angle of the transceivers is 25° . Based on these results, we can conclude that the LPL design is not suitable for underwater communication. These results demonstrate the effectiveness of CPL in combating device rotation in underwater communication.

Besides that, we also measure the BER when *Shrimp* adopts unpolarized light (i.e., without linear polarizer and waveplate) at various inclination angles. In this experiment, the distance between the transmitter and receiver is set as 0.8 m. As shown in Figure 12, we can see that unpolarized light is also not affected much by rotations. However, unpolarized light is still not a good candidate for underwater communication as it can be more severely affected by the ambient light which is also unpolarized. On the other hand, LPL and circularly polarized light are less affected⁸ by the ambient sunlight. As a result, to combat both device rotation and environmental interference in underwater communication, CPL is chosen.

- **Single Link vs. Double links.** To demonstrate the advantages of double CPL links over one single CPL link, we evaluate the performance difference in an indoor water pool with lights turned on. Here, *Shrimp* is respectively implemented with two links (two

⁸Note that even the circularly polarized light is affected less, the ambient light can still interfere the transmission.

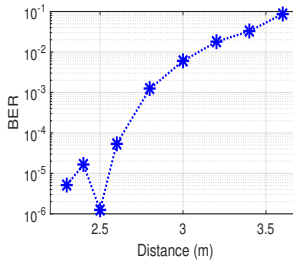


Figure 11: BER vs. distance in the outdoor sea water with fluctuating waves.

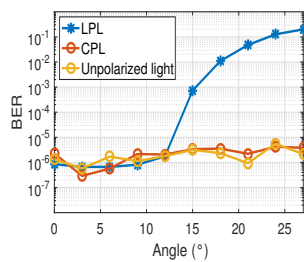


Figure 12: The effect of inclination angle on LPL, CPL, and unpolarized light.

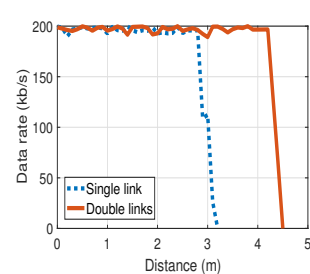


Figure 13: Single link vs. double links on the transmission distance.

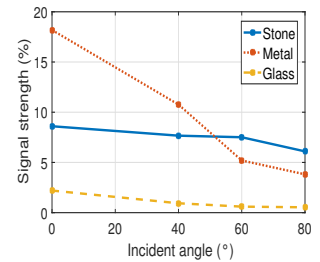


Figure 14: Signal strength of reflection from objects of different materials.

9 W LEDs) and a single link (one 18 W LED) to emit white light for communication. For single link, we employ OOK modulation. The transmission rates are both kept as 200 kbps. Note that in this experiment, we employ LEDs with a larger power input.

As shown in Figure 13, one link achieves a shorter communication distance. The reason is that when we only use a single link for underwater communication, it cannot combat ambient interference as it does not have two physically close-by links to remove the common interference. Therefore, the two link scheme outperforms the single link scheme in communication distance in underwater environment in the presence of ambient light interference.

5.5 NLoS Communication Through Reflections

We employ three obstacles made of different materials (stone, metal, and glass) to measure the reflection signal strengths at varying incident angles.⁹ As shown in Figure 14, the strength of the signal reflected by glass is the smallest, because the light signal can penetrate through the glass and only a small portion is reflected. For the metal obstacle, the strength of the reflected signal decreases rapidly as the incident angle increases. The reason is that the metal surface is smooth and thus specular reflection dominates. Hence, the obstacle can reflect a fraction of incident light and the reflected signal is relatively strong when the incident angle is small. Compared with metal, the surface of the stone is rough. Hence, most of the reflections are diffuse reflection, and the strength of the reflected signal does not change much at varying incident angles.

One important observation from this experiment is that VLC transceivers can still communicate with the help of reflection when the LoS link is blocked. This observation presents a new communication paradigm for visible light communication in complicated underwater environment. When the LoS link is blocked, two divers can still establish a communication link through reflection. In other words, in some extreme cases, objects can be utilized as a communication relay to enable NLoS communication. In our experiments, we have successfully realized music playing through reflection by pointing both transceivers towards a wall.

⁹Here, when the signal incident angle is perpendicular to the object surface, the incident angle is 0.

5.6 Effect of Seawater Depth

For experiments in the seawater (Figure 9(d)), we find that the water depth has an impact on the communication distance. This is mainly due to an interesting reason: during the photosynthesis process, chlorophyll is generated and chlorophyll can absorb the light signal. With the depth increases, the intensity of sunlight decreases and the photosynthesis becomes less. Therefore, in deeper seawater, the penetration capability of light signal is stronger. We present the testbed results (the red star) and simulation results (the blue line) in Figure 15.¹⁰ Note that the transmission power of our system is 15 W here. We can see that the experiment results match the simulation results quite well in the range of 0 - 5 meters. We hereby employ simulation to predict the communication distance in deeper water. With the increase of depth, the density of chlorophyll gradually drops, leading to a longer communication distance.

5.7 Human-Robot Communication

We evaluate the feasibility of underwater human-robot communication in this experiment as shown in Figure 9(h). We first measure the normalized signal power when the receiver is pointed at different orientations. In this experiment, the location of the transmitter (i.e., the robot) is fixed, which shines light at the receiver (i.e., diver). A 15 W LED is employed in this experiment. The location of the receiver is also fixed. Then we vary the receiver's orientation at different angles and measure the strength of the received signal.

The results are shown in Figure 16. We can see that the receiver has a broad coverage angle, approximately 140°. From the result, we can conclude that the signal is strong enough for data communication in a relatively large angle range. Therefore, the transmitter does not need to point the light signal exactly at the receiver for transmissions. The result demonstrates the flexibility of the proposed system.

5.8 Water-Air Communication

Another application scenario of our system is the water-air cross-media communication.

We first measure the signal strength obtained at the receiver at varying light incident angles with respect to the water-air interface.

¹⁰As our underwater robot can only work in water no deeper than 5 meters, we measure the system performance in water up to 5 meters.

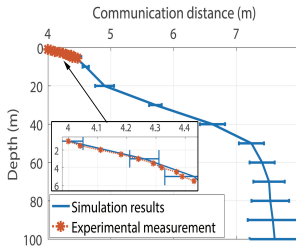


Figure 15: Effect of seawater depth on the communication distance.

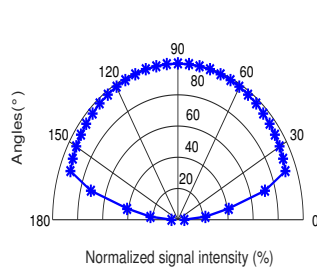


Figure 16: Signal strength when the receiver faces different orientations.

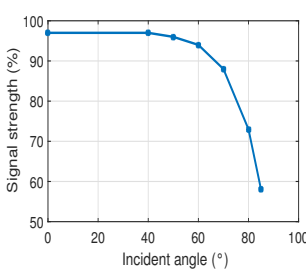


Figure 17: Effect of incident angle at the water-air interface on signal strength.

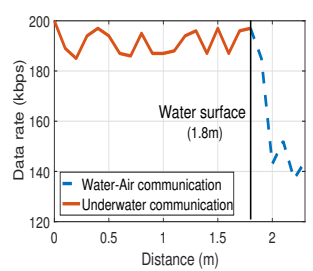


Figure 18: Water-water and water-air communication: the receiver is moved away from the transmitter.

As shown in Figure 17, when the incident angle is in the range of 0° and 40° , the signal loss rate caused by water reflection is low. Therefore, for water-air communication, it is not necessary to shine light signal vertically towards the surface of the sea, which provides convenience and flexibility. The only thing we need to pay attention to is to avoid the total reflection phenomenon [84].

We now evaluate the effect of air-water communication using blue light LED. At the beginning, both transmitter and receiver are placed 1.8 m below the water surface. Then the receiver is moved toward the water surface and eventually moved out of the water. We keep tracking the data rate during the process and the results are shown in Figure 18. We observe that, when both transmitter and receiver are under the water, a data rate around 190 kbps is achieved. However, when the receiver is just moved out of water, we observe a data rate decrease. We believe this is due to reflection at the water-air interface. After that, the data rate of water-air communication remains around 145 kbps.

6 Discussions

Shrimp leaves room for further investigation, as discussed below.

- **Improving the energy efficiency for light conversion.**

According to Malus's Law [43], after the light signal passes through a linear polarizer, the fraction of remaining energy is around 64% ($\int_0^{\frac{\pi}{4}} \cos^2 \theta d\theta \approx 64\%$), which means about 36% of energy is lost during this light conversion process. In fact, such energy loss can be reduced by using a specialized LED, which can directly emit polarized light, preserving more than 88.7% of energy [52].

- **Comparison with other underwater communication systems.**

We believe there is no single cure-all solution for underwater communication. Therefore, we should choose the right technology based on applications. The laser-based systems show merits in low power and high data rate. It can achieve higher than 2 Gbps rate with a power of just 0.5 W in a water pool as shown in Figure 19. However, it needs precise beam alignment between the transceivers. A good application scenario for laser-based approaches is when the transceivers can be placed at fixed locations such as the pool wall. On the other hand, if long distance is the main requirement, acoustic-based approaches may be the right option although the data rate is limited. For short distance transmission, our proposed system has advantages in terms of cost and reliability. We believe

there is still a large space to further improve the performance of the proposed system in terms of data rate and transmission range.

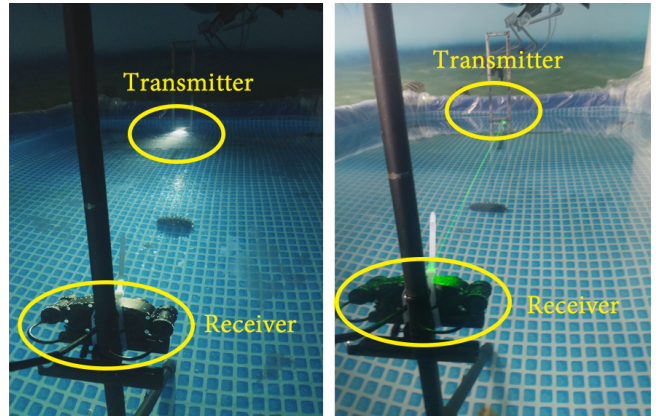


Figure 19: Underwater communication in a water pool: (a) *Shrimp* and (b) a laser-based communication system.

7 Related Work

Our system is broadly related to visible light communication and underwater communication.

- **Visible Light Communication.** Visible light communication (VLC) is a technology that enables high-speed connection between existing lighting infrastructure using LEDs [17, 18, 44, 78]. Considerable effort has been devoted to system designs including SmartLight [67], Strata [38], OpenVLC [6], and so on. Other research in this domain focuses on modulation capability [19, 73], throughput enhancement [58], programmable platform [18, 28], indoor sensing and positioning [7, 51, 59, 67, 85–87, 89], gesture recognition [8, 46, 76], vehicle networking [30, 45], low-power consumption [31], and so on. Although VLC in air has achieved a great success, there are still challenges when it is applied in underwater environment.

- **Underwater Communications.** In recent years, flourishing achievements have been obtained in developing highly efficient underwater communication techniques using different wireless technologies including RF signals [56], acoustic signals [69], and

so on. While promising progress has been achieved, the data rate is still limited [33, 68].

Different from the aforementioned signals, underwater optical wireless communication technology [29, 49, 70] provides a promising alternative which successfully addresses the data rate issue [84]. Laser communication has been applied in submarine-to-submarine communications [79], which can achieve long-distance and high throughput transmissions [36, 48]. However, laser-based approaches have a rigorous beam alignment requirement [82], making them not suitable for communication in complicated underwater environment.

A lot of effort has been devoted to the design of underwater VLC in terms of channel modeling [19, 40], propagation model [41, 71], modulation design [21, 37, 88], coding design [74], energy-saving [62, 73], interference resistance [16], polarization design [12, 24, 47, 54, 55, 61, 75], and so on. Furthermore, environmental factors, such as the salinity of water, absorption & scattering effect [9–11, 27, 32, 66, 81], retro-reflectors [22, 54], and fluctuations of waves [39, 83] are also taken into considerations when measuring the communication performance. Novel applications, such as air-water communication [15] and robot-robot communication [31, 34] are also discussed and tested. In a recent work [47], CPL-based VLC in air is proposed and evaluated. As a preliminary work, the modulation rate and achieved data rate are still low. The system is also not designed for underwater environment. The recent backscatter-based underwater acoustic communication system [35] achieves a throughput up to 20 kbps and a relatively long transmission range. Besides, optical-acoustic hybrid systems were also developed and explored [60].

In this work, we propose an interesting alternative *Shrimp*, which employs a double CPL design to achieve robust communication in underwater environment.

8 Conclusions

In this work, we design and implement *Shrimp*, a robust underwater VLC system. Circularly polarized light (CPL) with two opposite rotation directions is applied to address two issues in underwater communication: device rotation/displacement and dynamic sunlight interference. We implement transmitter and receiver with self-designed PCBs. Extensive experiments validate that *Shrimp* can effectively combat the environmental interference and achieve robust performance in underwater environments.

Acknowledgements

The authors would like to thank the anonymous reviewers and shepherd for their valuable comments and suggestions. This research is sponsored in part by the National Natural Science Foundation of China (61872052, 6202780103), Dalian Science and Technology Innovation Fund (2019J11CY004), and Science and Technology on Underwater Test and Control Laboratory (61424070506).

Appendix

In *Shrimp*, a prominent feature is the utilization of CPL. We present the related theoretical verifications below. At the transmitter end, the LED emits unpolarized light and its Stokes vector [57] is expressed as $S = [1 \ 0 \ 0 \ 0]^T$. Then, we use linear polarizers to convert

the unpolarized light into the 0° and 90° LPL, respectively. The calculations on Mueller matrices [23] and Stokes vectors [23, 57] (i.e., M and S) are presented below:

$$S_{0^\circ} = M_{0^\circ} S = \frac{1}{2} \begin{bmatrix} 1 & 1 & 0 & 0 \\ 1 & 1 & 0 & 0 \\ 0 & 0 & 0 & 0 \\ 0 & 0 & 0 & 0 \end{bmatrix} \begin{bmatrix} 1 \\ 1 \\ 0 \\ 0 \end{bmatrix} = \frac{1}{2} \begin{bmatrix} 1 \\ 1 \\ 0 \\ 0 \end{bmatrix}. \quad (1)$$

$$S_{90^\circ} = M_{90^\circ} S = \frac{1}{2} \begin{bmatrix} 1 & -1 & 0 & 0 \\ -1 & 1 & 0 & 0 \\ 0 & 0 & 0 & 0 \\ 0 & 0 & 0 & 0 \end{bmatrix} \begin{bmatrix} 1 \\ 1 \\ 0 \\ 0 \end{bmatrix} = \frac{1}{2} \begin{bmatrix} 1 \\ -1 \\ 0 \\ 0 \end{bmatrix}. \quad (2)$$

Afterwards, we use the quarter-wave plate to convert the LPL into two CPL of opposite directions: counterclockwise and clockwise. According to [63], for the counterclockwise CPL, its Stokes vector S_{CCW} is:

$$S_{CCW} = M_2 S_{90^\circ} = \frac{1}{2} \begin{bmatrix} 1 & 0 & 0 & 0 \\ 0 & 0 & 0 & -1 \\ 0 & 0 & 1 & 0 \\ 0 & 1 & 0 & 0 \end{bmatrix} \begin{bmatrix} 1 \\ -1 \\ 0 \\ 0 \end{bmatrix} = \frac{1}{2} \begin{bmatrix} 1 \\ 0 \\ 0 \\ -1 \end{bmatrix}. \quad (3)$$

M_2 is the Mueller matrix of the quarter-wave plate. Similarly, for the clockwise CPL, its Stokes vector S_{CW} is:

$$S_{CW} = M_2 S_{0^\circ} = \frac{1}{2} \begin{bmatrix} 1 & 0 & 0 & 0 \\ 0 & 0 & 0 & -1 \\ 0 & 0 & 1 & 0 \\ 0 & 1 & 0 & 0 \end{bmatrix} \begin{bmatrix} 1 \\ 1 \\ 0 \\ 0 \end{bmatrix} = \frac{1}{2} \begin{bmatrix} 1 \\ 0 \\ 0 \\ 1 \end{bmatrix}. \quad (4)$$

At the receiver end, upon receiving the double CPL, we use quarter-wave plate to convert them into LPL. The counterclockwise CPL can be converted as:

$$S_{0^\circ} = M_2 S_{CCW} = \frac{1}{2} \begin{bmatrix} 1 & 0 & 0 & 0 \\ 0 & 0 & 0 & -1 \\ 0 & 0 & 1 & 0 \\ 0 & 1 & 0 & 0 \end{bmatrix} \begin{bmatrix} 1 \\ 0 \\ 0 \\ -1 \end{bmatrix} = \frac{1}{2} \begin{bmatrix} 1 \\ 1 \\ 0 \\ 0 \end{bmatrix}. \quad (5)$$

Similarly, the clockwise CPL can be converted as LPL below:

$$S_{90^\circ} = M_2 S_{CW} = \frac{1}{2} \begin{bmatrix} 1 & 0 & 0 & 0 \\ 0 & 0 & 0 & -1 \\ 0 & 0 & 1 & 0 \\ 0 & 1 & 0 & 0 \end{bmatrix} \begin{bmatrix} 1 \\ 0 \\ 0 \\ 1 \end{bmatrix} = \frac{1}{2} \begin{bmatrix} 1 \\ -1 \\ 0 \\ 0 \end{bmatrix}. \quad (6)$$

Since the received LPL still contains noise (LPL of other angles), we use two linear polarizers (0° and 90°) to filter the noise. For Link 1, when the 0° LPL travels through a 0° linear polarizer, we have:

$$S' = M_{0^\circ} S_{0^\circ} = \frac{1}{2} \begin{bmatrix} 1 & 1 & 0 & 0 \\ 1 & 1 & 0 & 0 \\ 0 & 0 & 0 & 0 \\ 0 & 0 & 0 & 0 \end{bmatrix} \frac{1}{2} \begin{bmatrix} 1 \\ 1 \\ 0 \\ 0 \end{bmatrix} = \frac{1}{2} \begin{bmatrix} 1 \\ 1 \\ 0 \\ 0 \end{bmatrix}. \quad (7)$$

Equation (7) indicates that the optical signal can be successfully received, and LPL of other angles are filtered out. Similarly, for Link 2, a 90° LPL will go through a 90° polarizer. Based on the above verifications, we can obtain two LPL, the angles of which are orthogonal (0° and 90°) to each other, demonstrating the correctness and feasibility of the proposed system.

References

- [1] [n.d.]. AD620 Low Cost Low Power Instrumentation Amplifier. <https://www.analog.com/media/en/technical-documentation/data-sheets/AD620.pdf>.
- [2] [n.d.]. Cree XHP50 Data Sheet. <https://www.cree.com/led-components/media/documents/ds-XHP50.pdf>.
- [3] [n.d.]. Cree XHP70 Data Sheet. <https://www.cree.com/led-components/media/documents/ds-XHP70.pdf>.
- [4] [n.d.]. Cree XM-L Data Sheet. <https://www.cree.com/led-components/media/documents/XLampXMLEDW.pdf>.
- [5] [n.d.]. XL-Density Performance Line ARM®-based 32-bit MCU with 768 KB to 1 MB Flash, USB, CAN, 17 timers, 3 ADCs, 13 com. interfaces. <https://www.st.com/resource/en/datasheet/stm32f103rg.pdf>.
- [6] D. Juara A. Galisteo and D. Giustiniano. 2019. Research in Visible Light Communication Systems with OpenVLC1.3. In *IEEE WF-IoT*. 539–544.
- [7] D. Ahmetovic, F. Avanzini, A. Baratè, C. Bernareggi, G. Galimberti, L. A. Ludovico, S. Mascetti, and G. Presti. 2019. Sonification of Rotation Instructions to Support Navigation of People with Visual Impairment. In *IEEE PerCom*. 1–10.
- [8] C. An, T. Li, Z. Tian, A. T. Campbell, and X. Zhou. 2015. Visible Light Knows Who You Are. In *ACM VLCS@MobiCom*. 39–44.
- [9] D. Anguita, D. Brizzolara, and G. Parodi. 2009. **Building an Underwater Wireless Sensor Network based on Optical Communication: Research Challenges and Current Results**. In *IEEE SENSORCOMM*. 476–479.
- [10] D. Anguita, D. Brizzolara, and G. Parodi. 2010. VHDL Modeling of PHY and MAC Layer Modules for Underwater Optical Wireless Communication. In *IEEE ECCSC*. 185–188.
- [11] D. Anguita, D. Brizzolara, G. Parodi, and Q. Hu. 2011. **Optical Wireless Underwater Communication for AUV: Preliminary Simulation and Experimental Results**. In *IEEE OCEANS*. 1–5.
- [12] S. Benedetti and P. Poggiolini. 1992. Theory of Polarization Shift Keying Modulation. *IEEE Transactions on Communications* 40, 4 (1992), 708–721.
- [13] A. Bermak. 2019. Visible Light Communication System and Method. <https://www.freepatentsonline.com/y2019/0074901.html>
- [14] A. Bucholtz. 1995. Rayleigh-scattering Calculations for the Terrestrial Atmosphere. *Applied Optics* 34, 15 (1995), 2765–2773.
- [15] C. J. Carver, Z. Tian, H. Zhang, K. M. Odame, A. Q. Li, and X. Zhou. 2020. **AmphiLight: Direct Air-Water Communication with Laser Light**. In *USENIX NSDI*. 373–388.
- [16] A. Celik, N. Saeed, B. Shihada, T. Y. Al-Naffouri, and M. Alouini. 2020. End-to-End Performance Analysis of Underwater Optical Wireless Relaying and Routing Techniques Under Location Uncertainty. *IEEE Transactions on Wireless Communications* 19, 2 (2020), 1167–1181.
- [17] N. Cen, N. Dave, E. Demirors, Z. Guan, and T. Melodia. 2019. LiBeam: Throughput-Optimal Cooperative Beamforming for Indoor Visible Light Networks. In *IEEE INFOCOM*. 1972–1980.
- [18] N. Cen, J. Jagannath, S. Moretti, Z. Guan, and T. Melodia. 2019. LANET: Visible-light Ad Hoc Networks. *Ad Hoc Networks* 84 (2019), 107–123.
- [19] C. Chan, H. Tsai, and K. C. Lin. 2017. POLI: Long-Range Visible Light Communications using Polarized Light Intensity Modulation. In *ACM MobiSys*. 109–120.
- [20] M. Chandran and A. Anderson. 2011. Pulse Width Modulation based LED Dimmer Control. US Patent 7,990,081.
- [21] Ming Chen, Peng Zou, Long Zhang, and Nan Chi. 2019. Demonstration of A 2.34 Gbit/s Real-time Single Silicon-substrate Blue LED-based Underwater VLC System. *IEEE Photonics Journal* 12, 1 (2019), 1–11.
- [22] B. Cochenour, L. Mullen, W. Rabinovich, and R. Mahon. 2009. Underwater Optical Communications with A Modulating Retro-reflector. *Proceedings of Spie the International Society for Optical Engineering* 7317, 1 (2009), 1–10.
- [23] E. Collett. 2005. *Field Guide to Polarization*. Spie Bellingham, WA.
- [24] W. C. Cox, B. L. Hughes, and J. F. Muth. 2009. A Polarization Shift-keying System for Underwater Optical Communications. In *IEEE OCEANS*. 1–4.
- [25] W. C. Cox, J. A. Simpson, and J. F. Muth. 2011. Underwater Optical Communication using Software Defined Radio over LED and Laser based Links. In *IEEE MILCOM*. 2057–2062.
- [26] Y. Dong, X. Mi, and Y. Zhou. 2016. Spatial Channel Model for Underwater Wireless Optical Communication Links. In *ACM WUWNet*. 1–2.
- [27] M. Doniec and D. Rus. 2010. BiDirectional Optical Communication with AquaOptical II. In *IEEE ICCS*. 390–394.
- [28] W. Du, J. C. Liando, and M. Li. 2016. SoftLight: Adaptive Visible Light Communication over Screen-camera Links. In *IEEE INFOCOM*. 1–9.
- [29] M. Elamassie, F. Miramirkhani, and M. Uysal. 2018. Performance Characterization of Underwater Visible Light Communication. *IEEE Transactions on Communications* 67, 1 (2018), 543–552.
- [30] Maged Fakirah, Supeng Leng, Xiaosha Chen, and Jihua Zhou. 2020. Visible Light Communication-based Traffic Control of Autonomous Vehicles at Multi-lane Roundabouts. *Springer EURASIP Journal on Wireless Communications and Networking* 2020, 1 (2020), 1–14.
- [31] N. Farr, A. Bowen, J. Ware, C. Pontbriand, and M. Tivey. 2010. An Integrated, Underwater Optical/Acoustic Communications System. In *IEEE OCEANS*. IEEE, 1–6.
- [32] N. Farr, A. Chave, L. Freitag, J. Preisig, S. White, D. Yoerger, and P. Titterton. 2005. Optical Modem Technology for Seafloor Observatories. In *IEEE OCEANS*. IEEE, 928–934.
- [33] D. Frye, J. Ware, M. Grund, J. Partan, P. Koski, S. Singh, L. Freitag, J. Collins, and R. Detrick. 2005. An Acoustically-linked Deep-ocean Observatory. In *Europe Oceans*. 969–974.
- [34] Y. F. Fung, M. Dai, and M. F. Ercan. 2009. Underwater Short Range Free Space Optical Communication for a Robotic Swarm. In *IEEE ICARO*. 529–532.
- [35] R. Ghaffarivardavagh, S. S. Afzal, O. Rodriguez, and F. Adib. 2020. Ultra-Wideband Underwater Backscatter via Piezoelectric Metamaterials. In *ACM SIGCOMM*. 722–734.
- [36] F. Hansson and S. Radic. 2008. High Bandwidth Underwater Optical Communication. *Applied Optics* 47, 2 (2008), 277–283.
- [37] Salah Hessian, Sezer Can Tokgoz, Noha Anous, Ali Boyaci, Mohamed Abdallah, and Khalid A Qaraqe. 2018. Experimental Evaluation of OFDM-based Underwater Visible Light Communication System. *IEEE Photonics Journal* 10, 5 (2018), 1–13.
- [38] W. Hu, J. Mao, Z. Huang, Y. Xue, J. She, K. Bian, and G. Shen. 2014. Strata: Layered Coding for Scalable Visual Communication. In *ACM MobiCom*. 79–90.
- [39] M. V. Jamali, J. A. Salehi, and F. Akhoundi. 2017. Performance Studies of Underwater Wireless Optical Communication Systems With Spatial Diversity: MIMO Scheme. *IEEE Transactions on Communications* 65, 3 (2017), 1176–1192.
- [40] J. Jang and F. Adib. 2019. Underwater Backscatter Networking. In *ACM SIGCOMM*. 187–199.
- [41] S. Jaruwatanadilok. 2008. Underwater Wireless Optical Communication Channel Modeling and Performance Evaluation using Vector Radiative Transfer Theory. *IEEE Journal on Selected Areas in Communications* 26, 9 (2008), 1620–1627.
- [42] W. Jiang, T. Matsuda, K. Yatsui, and A. Tokuchi. 2002. MHz Pulsed Power Generator using MOSFET. In *IEEE Twenty-Fifth International Conference on Power Modulator Symposium*. 599–601.
- [43] Sönke Johnsen. 2012. *The Optics of Life: A Biologist's Guide to Light in Nature*. Princeton University Press.
- [44] A. Jovicic, J. Li, and T. Richardson. 2013. Visible Light Communication: Opportunities, Challenges and the Path to Market. *IEEE Communications Magazine* 51, 12 (2013), 26–32.
- [45] Lisa Kristiana, Arsyad Ramadhan Darlis, and Irma Amelia Dewi. 2020. The Feasibility of Obstacle Awareness Forwarding Scheme in A Visible Light Communication Vehicular Network. *International Journal of Electrical and Computer Engineering* 10, 6 (2020), 6453–6460.
- [46] T. Li, C. An, Z. Tian, A. T. Campbell, and X. Zhou. 2015. Human Sensing using Visible Light Communication. In *ACM MobiCom*. 331–344.
- [47] L. Liu. 2018. CPLC: Visible Light Communication based on Circularly Polarized Light. In *ACM ICICT*. 511–519.
- [48] L. Liu, S. Zhou, and J. Cui. 2008. Prospects and Problems of Wireless Communication for Underwater Sensor Networks. *Wireless Communications and Mobile Computing* 8, 8 (2008), 977–994.
- [49] X. Liu, S. Yi, X. Zhou, Z. Fang, Z. Qiu, L. Hu, C. Cong, L. Zheng, R. Liu, and P. Tian. 2017. 34.5m Underwater Optical Wireless Communication with 2.70 Gbps Data Rate based on a Green Laser Diode with NRZ-OOK Modulation. *Optics Express* 25, 22 (2017), 27937–27947.
- [50] X. Lu and J. Li. 2018. New Miller Codes for Run-Length Control in Visible Light Communications. *IEEE Transactions on Wireless Communications* 17, 3 (2018), 1798–1810.
- [51] J. Luo, L. Fan, and H. Li. 2017. Indoor Positioning Systems based on Visible Light Communication: State Of The Art. *IEEE Communications Surveys & Tutorials* 19, 4 (2017), 2871–2893.
- [52] E. Matioli, S. Brinkley, K. M. Kelchner, Y. Hu, S. Nakamura, S. DenBaars, J. Speck, and C. Weisbuch. 2012. High-brightness Polarized Light-emitting Diodes. *Light Science & Applications* 1, 8 (2012), 1–7.
- [53] T. Moore. 1974. Digital Transmission Codes: Properties of HDB3 and Related Ternary Codes with Reference to Broadcast Signal Distribution. *IET Radio and Electronic Engineer* 44, 8 (1974), 421–427.
- [54] L. Mullen, B. Cochenour, W. Rabinovich, R. Mahon, and J. Muth. 2009. Backscatter Suppression for Underwater Modulating Retroreflector Links using Polarization Discrimination. *Applied Optics* 48, 2 (2009), 328–337.
- [55] W. Niblack and E. Wolf. 1964. Polarization Modulation and Demodulation of Light. *Applied Optics* 3, 2 (1964), 277–279.
- [56] A. Palmeiro, M. Martin, I. Crowther, and M. Rhodes. 2011. Underwater Radio Frequency Communications. In *IEEE OCEANS*. 1–8.
- [57] N. G. Parker. 1949. Optical Algebra. *Journal of Mathematics and Physics* 28, 1 (1949), 131–139.
- [58] P. H. Pathak, X. Feng, P. Hu, and P. Mohapatra. 2015. Visible Light Communication, Networking, and Sensing: A Survey, Potential and Challenges. *IEEE Communications Surveys & Tutorials* 17, 4 (2015), 2047–2077.
- [59] N. Rajagopal, P. Lazik, and A. Rowe. 2014. Visual Light Landmarks for Mobile Devices. In *IEEE IPSN*. 249–260.
- [60] S. Han, Y. Noh, R. Liang, R. Chen, Y. Cheng, and M. Gerla. 2014. Evaluation of Underwater Optical-acoustic Hybrid Network. *China Communications* (2014),

- 49–59.
- [61] S. Pun, C. Chan, and L. Chen. 2005. A Novel Optical Frequency-shift-keying Transmitter Based on Polarization Modulation. *IEEE Photonics Technology Letters* 17, 7 (2005), 1528–1530.
 - [62] N. Saeed, A. Celik, T. Y. Al-Naffouri, and M. Alouini. 2019. **Localization of Energy Harvesting Empowered Underwater Optical Wireless Sensor Networks**. *IEEE Transactions on Wireless Communications* 18, 5 (2019), 2652–2663.
 - [63] S. N. Savenkov. 2009. Jones and Mueller Matrices: Structure, Symmetry Relations and Information Content. In *Light Scattering Reviews* 4. 71–119.
 - [64] G. W. Schmidt. 2000. Illumination Device using Pulse Width Modulation of a LED. US Patent 6,028,694.
 - [65] T. Shaneyfelt, M. A. Joordens, K. Nagothu, and M. Jamshidi. 2008. RF Communication between Surface and Underwater Robotic Swarms. In *2008 World Automation Congress*. 1–6.
 - [66] J. A. Simpson, B. L. Hughes, and J. F. Muth. 2012. Smart Transmitters and Receivers for Underwater Free-space Optical Communication. *IEEE Journal on Selected Areas in Communications* 30, 5 (2012), 964–974.
 - [67] L. Song and H. Tian. 2017. **Smartlight: Light-weight 3d Indoor Localization using A Single LED Lamp**. In *ACM SenSys*. 1–14.
 - [68] A. Stefanov and M. Stojanovic. 2011. Design and Performance Analysis of Underwater Acoustic Networks. *IEEE Journal on Selected Areas in Communications* 29, 10 (2011), 2012–2021.
 - [69] M. Stojanovic. 2007. On the Relationship between Capacity and Distance in an Underwater Acoustic Communication Channel. *ACM SIGMOBILE Mobile Computing and Communications Review* 11, 4 (2007), 34–43.
 - [70] M. Sui, X. Yu, and Z. Zhou. 2009. The Modified PPM Modulation for Underwater Wireless Optical Communication. In *IEEE ICCSN*. 173–177.
 - [71] S. Tang, Y. Dong, and X. Zhang. 2013. **Impulse Response Modeling for Underwater Wireless Optical Communication Links**. *IEEE Transactions on Communications* 62, 1 (2013), 226–234.
 - [72] F. Teixeira, J. Santos, L. M. Pessoa, M. Pereira, R. Campos, and M. Ricardo. 2015. Evaluation of Underwater IEEE 802.11 Networks at VHF and UHF Frequency Bands using Software Defined Radios. In *ACM WUWNET*. 16:1–16:5.
 - [73] Z. Tian, A. T. Campbell, and X. Zhou. 2015. Poster: Visible Light Communication in the Dark. In *ACM MobiCom*. 278–280.
 - [74] Sezer Can Tokgoz, Rubén Boluda-Ruiz, Serhan Yarkan, and Khalid A Qaraqe. 2019. ACO-OFDM Transmission over Underwater Pipeline for VLC-based Systems. In *IEEE PIMRC*. 1–7.
 - [75] H. Uehara, I. Seto, T. Ohtsuki, I. Sasase, and S. Mori. 1992. Phase Noise Insensitive Multilevel POLSK based on QAM Mapping in Coherent Optical Systems. In *IEEE ICOS/ISITA*. 1043–1047.
 - [76] A. Varshney, L. Mottola, and T. Voigt. 2018. Visible Light Communication for Wearable Computing. *CoRR* abs/1803.08583 (2018).
 - [77] H. Wang, L. Liu, and C. Lu. 2018. **CPLC: Visible Light Communication based on Circularly Polarized Light**. *Procedia Computer Science* 131 (2018), 511–519.
 - [78] Q. Wang, D. Giustiniano, and M. Zuniga. 2017. In Light and in Darkness, in Motion and in Stillness: A Reliable and Adaptive Receiver for the Internet of Lights. *IEEE Journal on Selected Areas in Communications* 36, 1 (2017), 149–161.
 - [79] T. Wiener and S. Karp. 1980. The Role of Blue/Green Laser Systems in Strategic Submarine Communications. *IEEE Transactions on Communications* 28, 9 (1980), 1602–1607.
 - [80] H. Wu, Q. Wang, J. Xiong, and M. Zuniga. 2020. **SmartVLC: Co-Designing Smart Lighting and Communication for Visible Light Networks**. *IEEE Transactions on Mobile Computing* 19, 8 (2020), 1956–1970.
 - [81] F. Xing, H. Yin, X. Ji, and V. C. M. Leung. 2020. **Joint Relay Selection and Power Allocation for Underwater Cooperative Optical Wireless Networks**. *IEEE Transactions on Wireless Communications* 19, 1 (2020), 251–264.
 - [82] F. Zafar, M. Bakaul, and R. Parthiban. 2017. Laser-diode-based Visible Light Communication: Toward Gigabit Class Communication. *IEEE Communications Magazine* 55, 2 (2017), 144–151.
 - [83] E. Zedini, H. M. Oubie, A. Kamoun, M. Hamdi, B. S. Ooi, and M. Alouini. 2019. **Unified Statistical Channel Model for Turbulence-induced Fading in Underwater Wireless Optical Communication Systems**. *IEEE Transactions on Communications* 67, 4 (2019), 2893–2907.
 - [84] Z. Zeng, S. Fu, H. Zhang, Y. Dong, and J. Cheng. 2016. **A Survey of Underwater Optical Wireless Communications**. *IEEE Communications Surveys & Tutorials* (2016), 204–238.
 - [85] C. Zhang and X. Zhang. 2018. Visible Light Localization using Conventional Light Fixtures and Smartphones. *IEEE Transactions on Mobile Computing* (2018), 2968–2983.
 - [86] C. Zhang, S. Zhou, and X. Zhang. 2016. Visible Light Localization using Incumbent Light Fixtures: Demo Abstract. In *ACM SenSys*. 304–305.
 - [87] J. Zhang, C. Zhang, X. Zhang, and S. Banerjee. 2016. Towards a Visible Light Network Architecture for Continuous Communication and Localization. In *ACM MobiCom*. 49–54.
 - [88] Ziyi Zhang, Yuanjia Lai, Junlong Lv, Pan Liu, Dongdong Teng, Gang Wang, and Lilin Liu. 2019. Over 700 MHz-3 dB Bandwidth UOWC System based on Blue HV-LED with T-bridge Pre-equalizer. *IEEE Photonics Journal* 11, 3 (2019), 1–12.